FULL PAPER

A Highly Elastic and Rapidly Crosslinkable Elastin-Like Polypeptide-Based Hydrogel for Biomedical Applications

Yi-Nan Zhang, Reginald K. Avery, Queralt Vallmajo-Martin, Alexander Assmann, Andrea Vegh, Adnan Memic, Bradley D. Olsen, Nasim Annabi, and Ali Khademhosseini**

Elastin-like polypeptides (ELPs) are promising for biomedical applications due to their unique thermoresponsive and elastic properties. ELP-based hydrogels have been produced through chemical and enzymatic crosslinking or photocrosslinking of modified ELPs. Herein, a photocrosslinked ELP gel using only canonical amino acids is presented. The inclusion of thiols from a pair of cysteine residues in the ELP sequence allows disulfide bond formation upon exposure to UV light, leading to the formation of a highly elastic hydrogel. The physical properties of the resulting hydrogel such as mechanical properties and swelling behavior can be easily tuned by controlling ELP concentrations. The biocompatibility of the engineered ELP hydrogels is shown in vitro as well as corroborated in vivo with subcutaneous implantation of hydrogels in rats. ELP constructs demonstrate long-term structural stability in vivo, and early and progressive host integration with no immune response, suggesting their potential for supporting wound repair. Ultimately, functionalized ELPs demonstrate the ability to function as an in vivo hemostatic material over bleeding wounds.

1. Introduction

Hydrogels have been widely used in biomedical applications for their potential to mimic characteristics of the extracellular matrix (ECM) environment present in native tissues.[1] The mechanical properties of hydrogel-based biomaterials are an important parameter in their design for biomedical applications. In particular, the elasticity of hydrogels plays a critical role in engineering soft and elastic tissues such as skin and blood vessels.[2] Synthetic polymeric hydrogels provide control over mechanical properties but capabilities such as cell adhesion and degradability must be further incorporated into the polymer.[3] On the other hand, many protein-based hydrogels intrinsically possess these properties and are promising

Y.-N. Zhang, R. K. Avery, Q. Vallmajo-Martin, Dr. A. Assmann, A. Vegh, Dr. A. Memic, Dr. N. Annabi, Prof. A. Khademhosseini
Biomaterials Innovation Research Center
Department of Medicine
Brigham and Women's Hospital
Harvard Medical School
Boston, MA 02139, USA
E-mail: n.annabi@neu.edu; alik@rics.bwh.harvard.edu

Y.-N. Zhang, Q. Vallmajo-Martin, Dr. A. Assmann, A. Vegh, Dr. A. Khademhosseini
Harvard-MIT Division of Health Sciences and Technology
Massachusetts Institute of Technology
Cambridge, MA 02139, USA

R. K. Avery
Department of Biological Engineering
Massachusetts Institute of Technology
Cambridge, MA 02139, USA

Q. Vallmajo-Martin
Laboratory for Cell and Tissue Engineering
Department of Obstetrics
University Hospital Zurich
Zürich CH-8091, Switzerland

Dr. A. Assmann, Dr. N. Annabi, Prof. A. Khademhosseini
Wyss Institute for Biologically Inspired Engineering
Harvard University
Boston, MA 02115, USA

Dr. A. Assmann
Department of Cardiovascular Surgery
Heinrich Heine University
40225 Duesseldorf, Germany

A. Vegh
Department of Materials Science and Engineering
University of Toronto
Toronto, Ontario M5S1A4, Canada

Dr. A. Memic
Center of Nanotechnology
King Abdulaziz University
Jeddah 21589, Saudi Arabia

Prof. B. D. Olsen
Department of Chemical Engineering
Massachusetts Institute of Technology
Cambridge, MA 02139, USA

Prof. N. Annabi
Department of Chemical Engineering
Northeastern University
Boston, MA 02115-5000, USA

Dr. A. Khademhosseini
Department of Physics
King Abdulaziz University
Jeddah 21569, Saudi Arabia

DOI: 10.1002/adfm.201501489

candidates for biomedical applications if their mechanical properties can be improved.

Protein-based hydrogels have been utilized for various biomedical applications due to their amino acid composition, supporting biocompatibility and potential ease of incorporation into the in vivo environment.[4–7] However, construction of protein-based hydrogels for biomedical applications requires crosslinking reactions to stabilize the hydrogels for in vivo applications.[8] Physical crosslinks, such as those observed in gelatin, chitosan, hyaluronic acid, and other natural polymers are sensitive to changes in temperature, pH or ionic concentrations.[5,6] These physically crosslinked hydrogels are capable of rapid gelation but require conditions unique to their mechanisms of crosslinking. Sometimes, these conditions are not present in vivo, thus compromising the applicability of these gels for some biomedical applications.[9]

In contrast, chemical crosslinking often results in permanent irreversible bonds between chemically active functional groups in the protein sequence.[10–13] Producing crosslinks between native groups such as amines, carboxyls, and sulfhydryls often requires the addition of a crosslinker, for instance, glutaraldehyde, to bind the aforementioned functional groups on amino acid residues.[12,14] The permanent bonds formed in chemically crosslinked systems can provide higher mechanical properties as compared to physically crosslinked hydrogels,[4] making these systems suitable for various biomedical applications.[5] However, long reaction times and generation of toxic byproducts in chemical crosslinking methods can, unfortunately, prevent their application in situations where rapid gelation in biological conditions is required. For example, carbodiimide-based coupling reactions commonly require minutes to hours to react and generate toxic byproducts,[15] which is not ideal for clinical applications. Enzymatic crosslinking of proteins also suffers from similar restrictions.[16]

Photocrosslinkable systems can overcome these limitations by forming chemical bonds within seconds or minutes to generate stable hydrogels.[17,18] Moreover, photocrosslinking allows for spatial and temporal control of crosslinking for in vitro and in vivo applications.[10–13,19] Photoactive functional groups such as benzophenones,[11] acrylate groups,[18] and nitrile groups,[6]can be chemically added to protein-based materials. These functionalized protein-based polymers can be crosslinked after a short UV exposure in the presence of a biocompatible photoinitiator to form stable hydrogels for both in vitro and in vivo applications.[4,11–13,20] One recent example is the formation of highly elastic hydrogels from methacryloyl-substituted tropoelastin (MeTro) which was shown to be biocompatible.[18] However, the addition of these functional groups to proteins is time-consuming and may cause batch-to-batch variations.

Elastin-like polypeptides (ELPs) are biopolymers that have been widely investigated for biomedical applications.[16,20,21] ELPs attempt to recapitulate the extensibility of natural elastin, which is an enzymatically crosslinked form of the tropoelastin monomer.[7,22] ELPs possess the elastic properties of elastin using a pentapeptide repeat: VPGXG where X is any amino acid besides proline. The unique properties of ELPs, including their reversible thermoresponsive nature,[23] modular designs,[13,24] mechanical properties,[16] and biocompatibility[7,20,25] make them suitable candidates for various applications such as thermoresponsive drug carriers, thermal purification components, self-assembly building blocks, and hydrogels for tissue regeneration.[16,20,26] ELPs have extensibility and thermal properties similar to the natural elastin protein, which is present in blood vessels, lung tissue, and other tissues that require continuous expansion and recovery over a lifetime.

Mechanical properties of ELPs are largely dependent on temperature and incorporated crosslinking sites.[27] Above the lower critical solution temperature, ELP agglomeration occurs, forming coacervates (viscous liquids), that can be used as cell carriers or injectable delivery systems.[7] For the formation of more stable gels, chemical crosslinking of ELPs is pursued. ELPs can be crosslinked through chemical functionalization of the protein sequence (e.g., addition of vinyl groups) by using glutaraldehyde, carbodiimide reactions,[10,12,28] or through the reaction of amines or carboxyl groups in the protein.[13,16,20,21,27] Chemical modifications can introduce well-defined concentrations of crosslinkers per molecule, providing control over both the location and amount of added crosslinkable groups. Noncanonical amino acids can also be recombinantly incorporated to provide photocrosslinkable sites within the protein.[29] In addition, photocrosslinking of ELPs has been performed with the addition of acrylate moieties to lysine groups.[30] Similar strategies have been used to form MeTro gels with tunable elasticity and stiffness.[18] However, acrylation reactions are time-consuming (can require up to 24 h) and may yield varied degrees of functionalization between batches, affecting the amount of available crosslinking sites and the resulting mechanical properties.

In this project, we aimed to harness the modularity of recombinant protein expression to design photocrosslinkable ELPs with improved extensibility without any chemical functionalization or incorporation of noncanonical amino acids. We hypothesized that improved mechanical properties can be achieved by designing a polypeptide containing thiol residues. Chain extension by disulfide bonds has been shown to improve extensibility and toughness of protein-based hydrogels.[31] Placing crosslinking sites at the ends of the protein is hypothesized to result in consistent molecular weight between crosslinks and a conservation of the elastic properties of ELPs. We anticipate that utilizing the ELP sequence outlined here, in addition to the modularity of recombinant expression, can generate rapidly gelling, extensible, and biocompatible ELP-based biomaterials.

2. Results and Discussion

2.1. ELP Design and Expression

The sequence expressed for the formation of photocrosslinkable ELP gels had 70 repeats of the pentapeptide sequence, VPGVG, in which every fifth pentapeptide replaced the first valine with an isoleucine (i.e., $[[VPGVG]_4IPGVG]_{14}$). Two peptide forms were expressed: one with the residues Lys-Cys-Thr-Ser (KCTS) flanking the ELP sequence (named KCTS-E_{31}-KCTS) and a second without any flanking residues (named as E_{22}) (**Figure 1**a). Flanking sequences containing cysteine residues were chosen for their potential to promote chain extension and improve the mechanical properties of the resulting hydrogel.[31] The proteins were

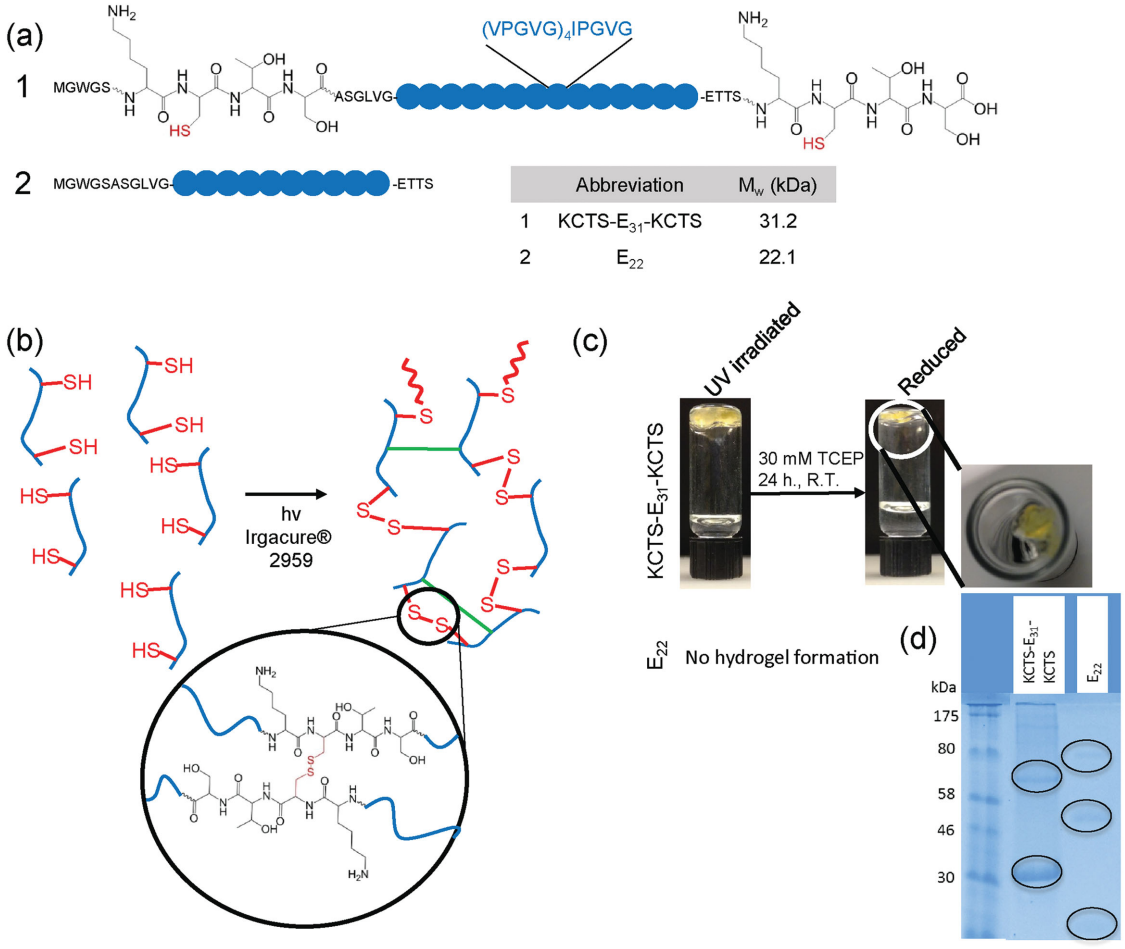

Figure 1. Design and photocrosslinking of elastin-like polypeptides (ELPs). a) Sequences of expressed ELPs to test photocrosslinking. b) Proposed photocrosslinking mechanism for cysteine-containing ELP (KCTS-E_{31}-KCTS), involving chain extension via disulfide bond formation (red bonds) and interchain crosslinking among ELP residues (green bonds). c) Representative images of 10 % (w/v) aqueous ELP solutions after UV exposure in the presence of a photoinitiator and after incubation with a reducing agent, tris (2-carboxyethyl) phosphine hydrochloride (TCEP). KCTS-E_{31}-KCTS forms a gel after photocrosslinking while E_{22}, an ELP lacking cysteine residues, remains a liquid. After reduction, KCTS-E_{31}-KCTS is much smaller in size suggesting a mass loss after reduction. d) Protein electrophoresis gels of reduced hydrogels show bands (circled on gel), at double and triple the protein molecular weight when compared to nonreduced gels, indicating high molar mass proteins and the presence of some bonds other than disulfide bonds forming during photocrosslinking.

expressed in *Escherichia coli* (*E. coli*) hosts, followed by lysis and purification by inverse transition cycling.[23] Briefly, ELP solutions were alternatively equilibrated and centrifuged above (37 °C) and below (4 °C) their thermal transition temperature (T_t = 29 °C in 1% (w/v) solution) (Figure S1, Supporting Information). Because the ELP protein precipitates at high temperature and is solubilized at low temperatures, these temperature changes can provide a way to collect and purify the ELP proteins. Solutions of purified proteins were then dialyzed against water, lyophilized and stored at room temperature until use. Yields of pure ELP (purity >90%) (Figure S1, Supporting Information) were 1 g L^{-1} for 5 L fermentations, with purity confirmed by gel electrophoresis.

2.2. Photocrosslinking of ELP

Our experiments confirm that only cysteine-containing ELPs, KCTS-E_{31}-KCTS, could be photocrosslinked and form elastic gels following exposure to UV light in the presence of a photoinitiator, Irgacure® 2959 (Figure 1b). Stable gels were formed between 30 s to 3 min of irradiation depending on their volume based on the inversion test (Figure 1c). Thiols, present in KCTS-E_{31}-KCTS, are generally used in radical polymerizations as chain transfer agents.[32] In polymerizations, they serve to transfer radicals to initiate new chains.[19] However, in the crosslinking of KCTS-E_{31}-KCTS, it is hypothesized that the presence of thiols performs two functions: a) produces disulfide bonds and b) results in chain extension[31] of the ELP. Following irradiation of the photoinitiator, radicals react first with the sulfhydryl groups, which have the lowest binding dissociation energy in the peptide system.[32,33] Further crosslinking among residues or backbone groups of the ELP must also occur to produce a hydrogel network, as two cysteine residues per protein would only result in chain extension. Crosslinks among ELP residues are presumed to occur by transfer of radicals from the photoinitiator, leading to a stable hydrogel network.

To confirm these hypotheses, ELPs containing cysteines (KCTS-E_{31}-KCTS) and ELPs containing only the pentapeptide repeat (E_{22}) were irradiated under identical conditions. Gels were only formed in KCTS-E_{31}-KCTS samples, indicating the inability of the residues in the E_{22} sequence alone to form a photocrosslinked gel. Next, to determine the nature of these crosslinks, photocrosslinked KCTS-E_{31}-KCTS ELP gels were incubated in 30×10^{-3} M tris (2-carboxyethyl) phosphine hydrochloride (TCEP) solution as an irreversible reducing agent to break disulfide bonds. This procedure resulted in almost complete dissolution of the gel (Figure 1c), suggesting disulfide bond formation is a factor, but not the only source, of crosslinks in the system. Gel electrophoresis bands around double the molecular weight of KCTS-E_{31}-KCTS and E_{22} were observed after irradiation and complete reduction, indicative of chemically crosslinked ELP dimers (Figure 1d). Their presence, even after reduction in an excess of reducing agent, indicates that some crosslinking, other than disulfide bonds, persisted in the reduced photocrosslinked ELPs. The nature of these crosslinks is unclear, but is believed to involve peroxyl formation in an oxygen rich environment and hydrogen abstraction from peptide or backbone residues.[34,35] It is speculated that additional radicals, formed by hydrogen abstraction from ELP residues[33,34] were produced by radical transfer from the photoinitiator. There was a threefold molar excess of photoinitiator in the system compared to thiol groups, providing sufficient radicals even after reaction of all thiol groups. It is hypothesized that additional crosslinks between moieties (C—H, O—H, or N—H groups) in the ELP sequence occurred due to the radical transfer from the excess photoinitiator and these crosslinks were not reduced when incubated in a reducing agent. The combination of disulfide bond formation and the crosslinking of ELP residues resulted in a covalently crosslinked elastic hydrogel.

2.3. Physical Characterization

2.3.1. Pore Size and Swelling Ratios of Photocrosslinked ELP Hydrogels

The porosity of biomaterials plays an important role in their interaction with cells and newly formed tissues.[36] Controlling porosity and microarchitectural features in hydrogels enables the creation of engineered tissues with structures and functions similar to native tissues.[36] In addition, cellular penetration and new tissue formation within the 3D structures of these hydrogels are significantly improved by increasing the porosity.[37]

The ELP concentration significantly influenced both pore characteristics and swelling behavior of the fabricated ELP hydrogels. The apparent pore size of the ELP hydrogels decreased from 4.70 ± 0.48 μm to 1.58 ± 0.24 μm and 1.53 ± 0.20 μm as the ELP concentrations increased from 10% to 15%, and 20% (w/v), respectively (**Figure 2**a–d) ($p < 0.0001$ between 10% and 15%, 10%, and 20% (w/v)). The engineered ELP hydrogels had a denser microstructure compared to chemically

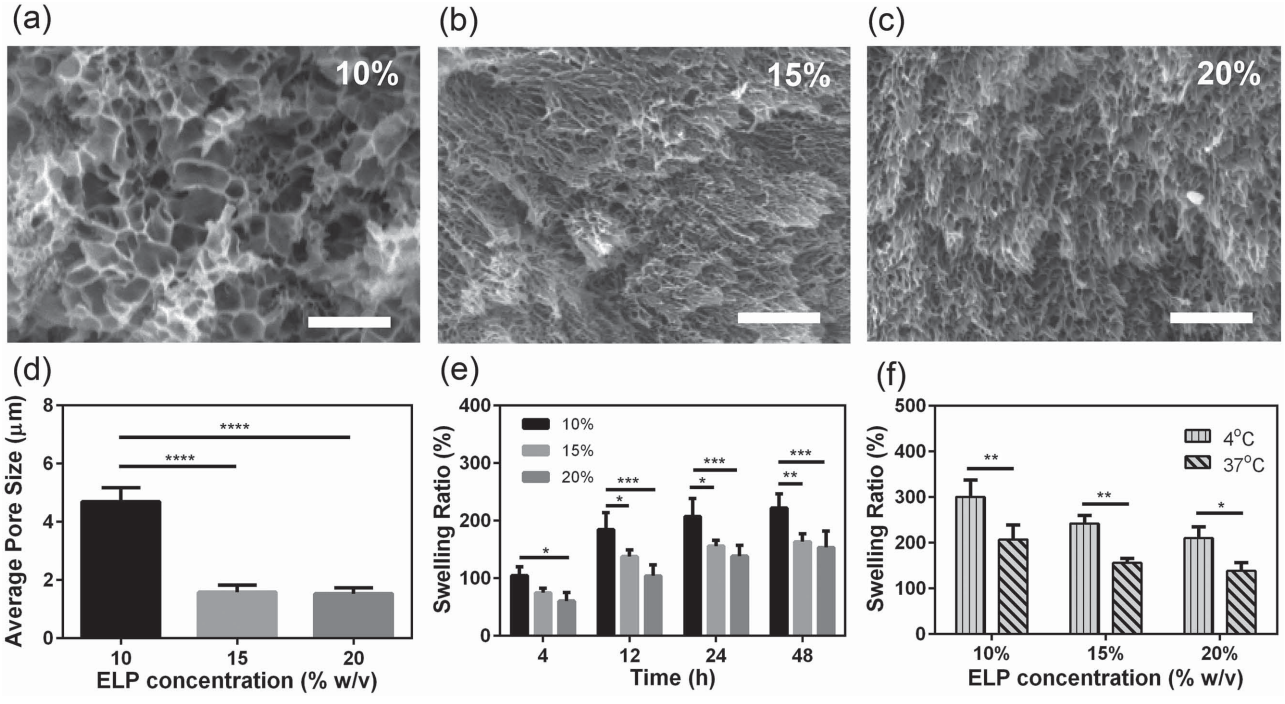

Figure 2. Pore characteristics and swelling properties of photocrosslinked ELP hydrogels. Representative SEM images from the cross sections of ELP hydrogels produced by using a) 10, b) 15, and c) 20% (w/v) ELP concentrations (scale bar = 10 μm). The structure of these hydrogels became more compact by increasing ELP concentration. d) Effect of protein concentrations on the average apparent pore sizes of ELP gels, derived from SEM images. The apparent pore size decreases by increasing the protein concentration. e) Time course of the swelling ratio depending on different ELP concentrations at 37 °C. f) Swelling ratio after 24 h depending on temperature and ELP concentrations show the thermoresponsive property of the photocrosslinked ELP gels (*$p < 0.05$, **$p < 0.01$, ***$p < 0.001$, ****$p < 0.0001$).

crosslinked ELPs[38] and UV crosslinked MeTro.[18] Maximum swelling ratios were reached after 24 h at 207 ± 32%, 156 ± 10%, and 138 ± 19% for ELP concentrations of 10%, 15%, and 20% (w/v), respectively (Figure 2e). In addition, the fabricated ELP hydrogels responded to temperature changes even after crosslinking. For example, there was a significant increase ($p < 0.01$) in the swelling ratios up to 1.5-fold for 10% (w/v) ELP hydrogels when the swollen hydrogels were transferred from 37 °C to 4 °C (Figure 2f). Higher ELP concentrations provide increased crosslinking density, which can lead to reduction in swelling ratio and pore size.[38]

2.3.2. Mechanical Properties of ELP Hydrogels

Tensile tests on photocrosslinked KCTS-E_{31}-KCTS hydrogels showed high extensibility (up to 420%) and tunable tensile strength by changing ELP concentrations (**Figure 3**a,b). The ultimate strain at fracture was determined to be 419 ± 25%, 395 ± 10%, and 388 ± 12% for ELP concentrations of 10%, 15%, and 20% (w/v), respectively (Table S1, Supporting Information). The extensibility of ELP gels were similar to MeTro gels (with extensibility up to 400%)[18] and much higher than a previously fabricated ELP-collagen hydrogel (up to 80%) and other types of ELPs (ranging from 80% to 120%).[39]

The extensibility of a native pulmonary artery varies from 158 ± 25% to 282 ± 48% depending on the direction of tensile loading; thus the crosslinked ELPs developed here are capable of withstanding extensions in excess of those achieved in arterial tissue.[18,37] The fabricated hydrogels showed elastic moduli of 1.28 ± 0.17 kPa, 1.72 ± 0.11 kPa, and 2.21 ± 0.36 kPa ($p < 0.05$ between 10% and 15% (w/v), $p < 0.01$ between 15% and 20% (w/v), and $p < 0.0001$ between 10% and 20% (w/v)) and ultimate tensile strengths of 6.46 ± 0.35 kPa, 7.71 ± 0.53 kPa, and 10.09 ± 1.81 kPa for ELP gel concentrations of 10%, 15%, and 20% (w/v) (Figure 3b,c, Table S1, Supporting Information). Higher ELP concentrations can provide increased crosslinking density, which may increase the hydrogel stiffness. This is corroborated by the trends observed in the swelling ratio and pore size.[38] Increasing ELP concentrations from 15% to 20% (w/v) did not significantly change the apparent pore size as shown in Figure 2d but the mechanical properties were significantly increased (Figure 3). We hypothesize that the ELP gels may reach their maximum crosslinking density at 15% (w/v) ELP; therefore, further increases in ELP concentration will not change the pore size. However, higher concentrations of equally photocrosslinked gels will result in increased mechanical properties because of additional physical interactions (aggregation) among the ELP chains. Both the elastic moduli and tensile strength showed lower values compared to the MeTro gels (2.8–14.8 kPa)[18] and ELP-collagen hydrogels (20 kPa),[40] as a result of having only two disulfide bonds per chain in addition to the random radical crosslinking among ELP residues. The unique elastic properties of this photocrosslinkable ELP hydrogel result in its potential use for the engineering of elastic tissues such as blood vessels, skin, lung, or cardiac tissues due to the important role of elasticity for the function of these tissues.[18,37]

Cyclic compression of the ELPs showed complete recoverability of the gel after multiple cycles of compression (Figure 3d–f). As shown in Figure 3d, the ELP hydrogels deformed reversibly following 10 cycles of loading and unloading, with compression up to ≈70% strain. The compressive moduli were 3.01 ± 0.44 kPa, 6.15 ± 0.28 kPa, and 13.05 ± 1.2 kPa when the ELP concentration was increased from 10%, 15%, to 20% (w/v) (Figure 3e, Table S1, Supporting Information) ($p < 0.01$ between 10% and 15% (w/v), $p < 0.0001$ between 15% and 20%, 10% and 20% (w/v)), which follows the trends from tensile testing (Figure 3c). The compressive modulus of the photocrosslinked ELPs shows similar values to a chemically crosslinked ELP[KV_7F-72] (4-11 kPa) developed by Lim et al.,[38] but it is lower than MeTro gels (9-160 kPa) as reported in our previous study.[18] Energy loss based on cycle 8 was found to be 35.13 ± 2.55%, 42.10 ± 4.37%, and 51.15 ± 2.90% for 10%, 15%, and 20% (w/v) ELP hydrogels (Figure 3f, Table S1, Supporting Information) ($p < 0.01$ between 10% and 20% (w/v), $p < 0.05$ between 15% and 20% (w/v)). Previous studies showed that other hydrogels such as hybrid alginate/polyacrylamide gels exhibited high hysteresis and permanent deformation after cyclic loading, with some weakening after the second cycle of compression.[41] Despite high energy dissipation during loading/unloading, the minimal fatigue observed in photocrosslinked KCTS-E_{31}-KCTS hydrogels after compressive loading confirmed that the elastic nature of ELP gels is preserved after repeated deformations, necessary for implants such as those for cartilage or intervertebral discs.[20]

2.4. Cell Interactions

Photocrosslinked ELP gels enabled the growth and proliferation of mesenchymal stem cells (MSCs) and human umbilical vein endothelial cells (HUVECs), suggesting their biocompatibility. MSCs and HUVECs were chosen for in vitro tests for their important role in vascular tissue engineering. Because of their high extensibility, ELP gels are potential candidates for engineering elastic tissues such as blood vessels.[42,43] Both cells were cultured on the surface of 10% (w/v) photocrosslinked ELP hydrogels for 7 days. Cellular viability, metabolic activity and attachment were assessed for both MSCs (**Figure 4**a,b, Figure S2a, Supporting Information) and HUVECs (Figure 4c,d, Figure S2b, Supporting Information). Cell viability was higher than 80% on ELP hydrogels 1, 4, and 7 days after seeding (Figure 4a,c), suggesting that the engineered ELP gels had no cytotoxicity with either MSCs or HUVECs.

The capacity of the ELP hydrogel surface to support cellular proliferation was supported by cell viability maintenance up to 7 days. Furthermore, cell activity was also shown to increase over time for both cell types ($p < 0.0001$). MSCs showed higher metabolic activity than HUVECs due to their intrinsic higher cellular metabolic rate.[44] However, cell spreading was limited for both cell types (Figure S2c, Supporting Information). This is likely due to the lack of cell recognition sites such as arginine-glycine-aspartic acid peptides (RGD) in the ELP sequence, which can promote cell adhesion and spreading.[13,45] Based on previous studies, by modification of the ELP sequence with the addition of RGD, cell affinity and spreading can be improved.[13,46] For example, Costa et al. reported that ELP-RGD coated surfaces significantly enhanced cell adherence as

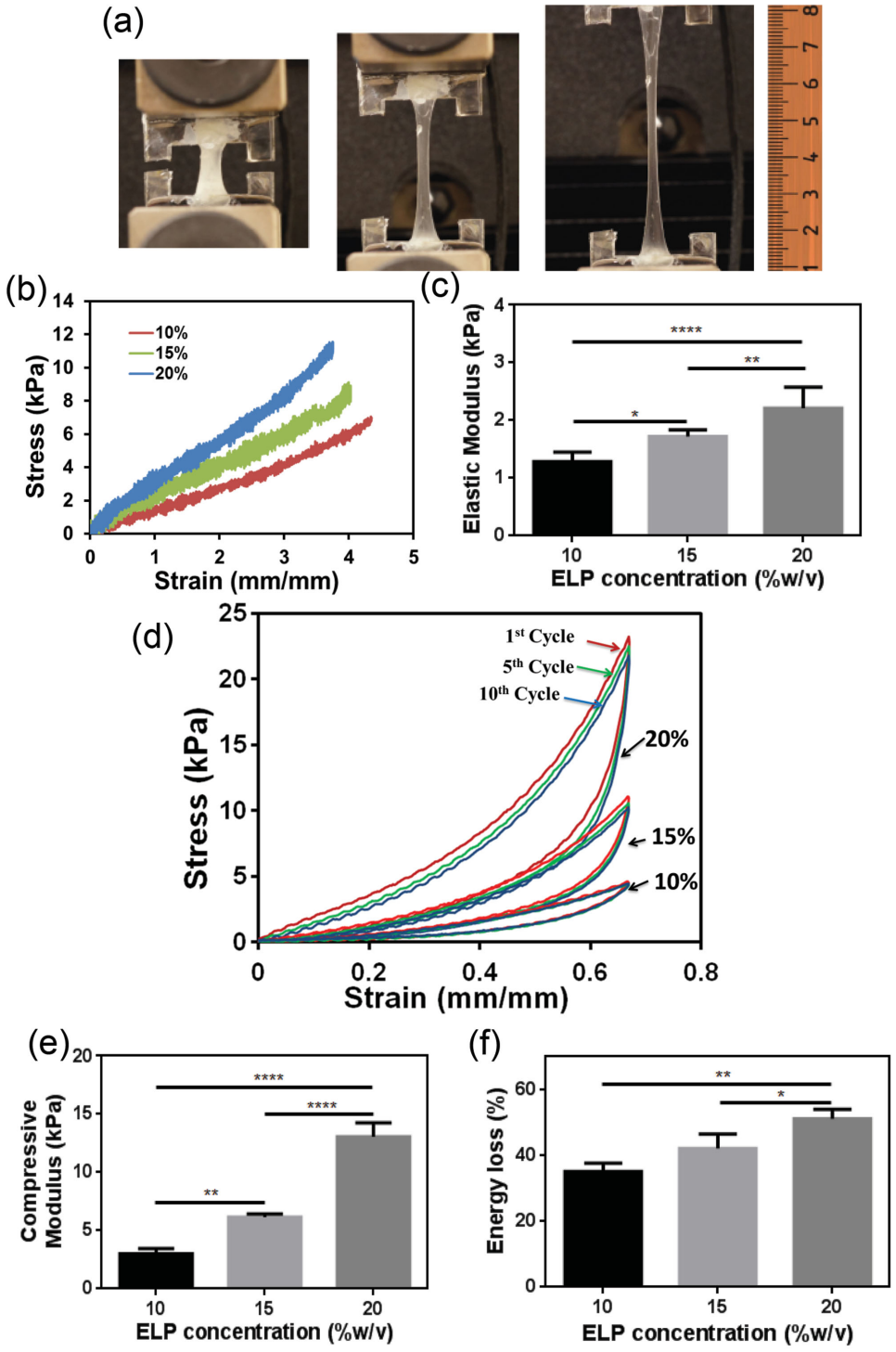

Figure 3. Mechanical properties of ELP hydrogels. a) Images of a 10% (w/v) ELP hydrogel during stretching. b) Representative tensile stress–strain curves. The engineered ELP hydrogel stretched more than four times its initial length before fracture. c) Elastic modulus of hydrogels produced with different ELP concentrations. d) Representative compressive cyclic loading and unloading curves for ELP hydrogels with different ELP concentrations show minimal fatigue. e) Compressive modulus of hydrogels produced with different ELP concentrations. f) Energy loss calculated from the area between the loading and unloading curves for 10%, 15%, and 20 % (w/v) gels (*$p < 0.05$, **$p < 0.01$, ****$p < 0.0001$).

compared to surfaces coated with just an ELP monolayer.[46] Raphel et al. have also reported that cells adhered more rapidly with a significant enhancement in cell spreading on an ELP-RGD surface compared to a non-RGD ELP control.[13] In our study, the aim was to use the engineered KCTS-E_{31}-KCTS gels as hemostatic materials for wound closure, where cell

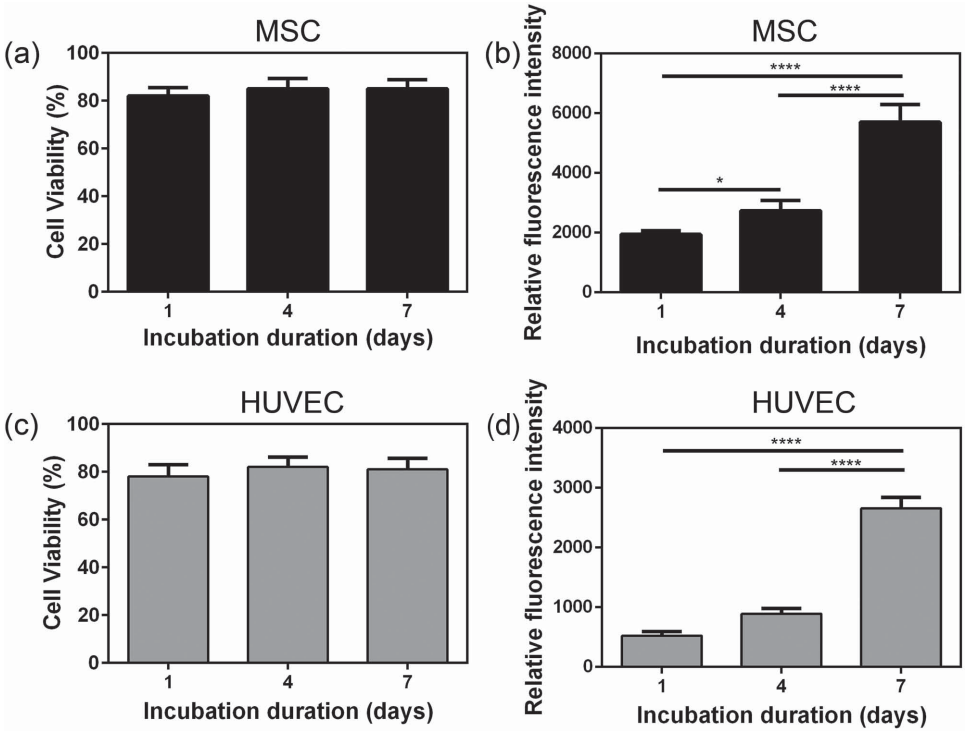

Figure 4. In vitro cell seeding on ELP hydrogels. a) Viability results and b) quantification of metabolic activity by PrestoBlue 1, 4, and 7 days after seeding with MSCs. c) Viability results and d) quantification of metabolic activity by PrestoBlue 1, 4, and 7 days after seeding with HUVECs (*$p < 0.05$, ****$p < 0.0001$).

spreading on ELP gels is not required.[45] For future tissue engineering applications of these ELP hydrogels, RGD modification can be easily performed as explained in previous studies.[45–47]

2.5. Biodegradation and Biocompatibility of ELP Hydrogels In Vivo

ELP gels were subcutaneously implanted in rats to assess gel stability and local interaction of the implant with the animal tissue as well as the immune response of the host. Harvesting of ELP samples at days 7, 14, 28, and 56 revealed maintained macroscopic shapes of the implants during the entire study period, suggesting no relevant degradation of the gels (**Figure 5**a). A slight decrease in gel diameter between day 0 and 7 compared to the other time points was observed, which might be due to shrinkage of the samples after implantation. This is explained by a combination of the thermoresponsive change in swelling ratios from room temperature to 37 °C and the loss of the in vitro swelling buffer into the subcutaneous pocket. The dry weight of the explanted samples was stable during the first four weeks, while the weight was significantly ($p < 0.001$) increased at eight weeks (Figure 5b). Constant weight may be explained by lack of degradation, whereas an increase in weight after eight weeks may be due to tissue ingrowth in the ELP construct. Indeed, hematoxylin and eosin staining of subcutaneous ELP implants showed early and progressive ingrowth of predominantly non-inflammatory tissue from the recipient into the samples, implying biocompatibility and integration of the ELP hydrogels in vivo (Figure 5c). Lack of degradation of ELP hydrogels was further corroborated by in vitro studies in which equilibrated 10%, 15%, and 20% (w/v) gels were incubated with the digestion enzyme Proteinase K (0.5 µm mL^{-1}) for 6 h (Figure S3, Supporting Information). Gels had only degraded 20% at 6 h, showing very slow degradation compared to other hydrogels following a similar crosslinking mechanism.[48] Moreover, previous publications have reported slow degradation rates for poly(VPGXG) ELPs.[49] In addition, mild ingrowth of tissues was observed when the crosslinked ELP hydrogels were implanted in the knee defects of rabbits.[20,50] Considering potential future applications of the material, the characteristics of slow implant degradation and tissue ingrowth are beneficial properties. Slow degradation allows for substantial cellular ingrowth and replacement of the implant by autologous neo-tissue. In order to adequately seal an internal tissue defect or stop a hemorrhage, it is crucial that the material is not degraded before autologous wound healing tissue has replaced the implant.[49,50] Many biomedical applications, for example, as surgical sealants or hemostats, could benefit from materials with these properties.[37,43,51–53]

Thorough evaluation of the histology, samples did not reveal a relevant amount of mononuclear inflammatory cells, which would have been typical from a strong local immune response by the host (Figure 5c). Corroborating this observation, immunohistological staining against surface markers of inflammatory cells proved that there was no lymphocyte infiltration (CD3), neither in the samples nor in the surrounding subcutaneous tissue. Additionally, mild macrophage invasion (CD68) into the interface zone between the sample and the host tissue was observed at day 7, but it completely disappeared by day

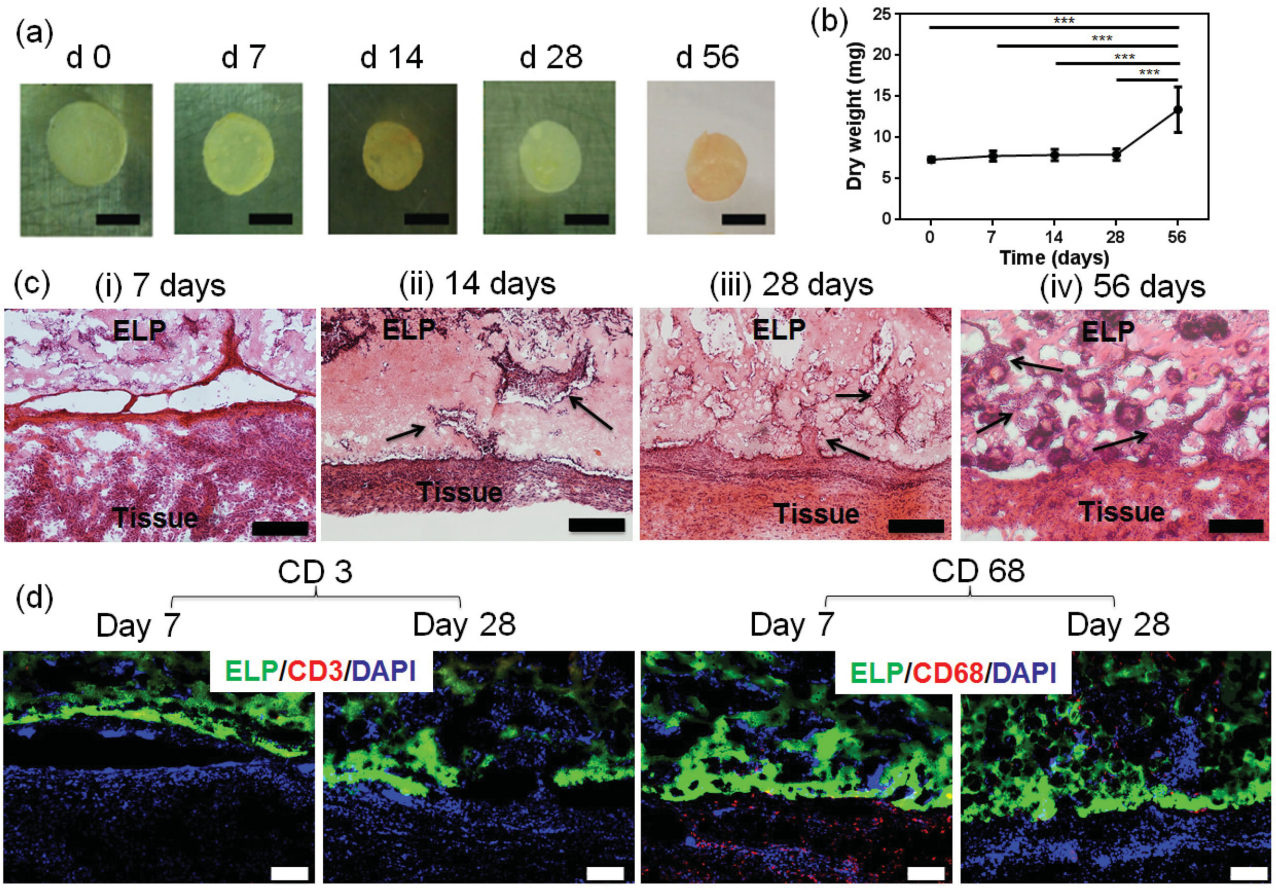

Figure 5. Evaluation of degradation and biocompatibility of ELP hydrogels in vivo. ELP hydrogels were implanted into the dorsal subcutaneous space of rats. a) Macroscopic view on explanted ELP hydrogels 0, 7, 14, 28, and 56 d after implantation (scale bar = 5 mm). b) The in vivo degradation profile of ELP hydrogels ($n = 5$) over time based on dry weight measurements shows a significant gain in weight at day 56. c) Hematoxylin/eosin staining of subcutaneously implanted ELP hydrogels at postoperative days i) 7, ii) 14, iii) 28, and iv) 56 revealed progressive growth of host tissue into the implants, shown by the arrows (scale bar = 200 μm). d) Immunostaining of subcutaneously implanted ELP hydrogels at day 7 and 28 resulted in no local lymphocyte infiltration (CD3), and relevant macrophage detection (CD68) only at day 7, having disappeared by day 28 (scale bar = 100 μm). Green color in (d) represents the autofluorescent ELP, red color the immune cells, and blue color all cell nuclei (DAPI) (***$p < 0.001$).

28 (Figure 5d). This is in contrast to many commercial tissue sealants and hemostats, which evoke considerable inflammatory host response especially in terms of macrophage infiltration at implantation sites.[54,55]

2.6. Hemostatic potential of ELP hydrogels In Vitro and In Vivo

Given the stability and biocompatibility of the engineered ELPs, an investigation of their potential as an elastic hemostatic material was performed. Hemostatic materials are used in surgical, emergency, and combat situations to manage uncontrolled bleeding by multiple mechanisms.[56] Release of clotting factors, absorption of fluid, and sealing are all hemostatic mechanisms.[51] An advantage of absorbent, sealing, or adhesive hemostatic materials is their independence from the clotting cascade, which can be compromised in some patients. The physical barrier formed by the hemostatic materials can staunch blood loss while the body progresses toward hemostasis.[52,55,57] The use of colloidal solutions of silica nanoparticles (NPs) as hemostatic agents and tissue adhesives has been recently demonstrated.[58,59] These solutions function to bind tissues together, in a process termed nanobridging, forming effective hemostatic seals in the presence of blood. Nanobridging occurs when NPs in solution form connections that can adhere tissues together.[58] However, as colloidal solutions, delivery to a wound would be suboptimal due to their ability to flow away from the injury site. Using a flexible substrate to deliver a coating of colloidal particles will 1) provide control over the concentration of colloidal solution delivered to a wound based on surface area, 2) maintain intimate contact between the colloidal particles and the wound site, and (3) provide an elastic substrate responsive to mechanical deformations of the wounded tissue. Here, we combine the ELPs with colloidal solutions of NPs and test their hemostatic potential (**Figure 6**a).

2.6.1. In Vitro Clotting Time Assay

The addition of silica NPs as a colloidal solution (50 % (w/v)) on the surface of photocrosslinked KCTS-E_{31}-KCTS ELP resulted

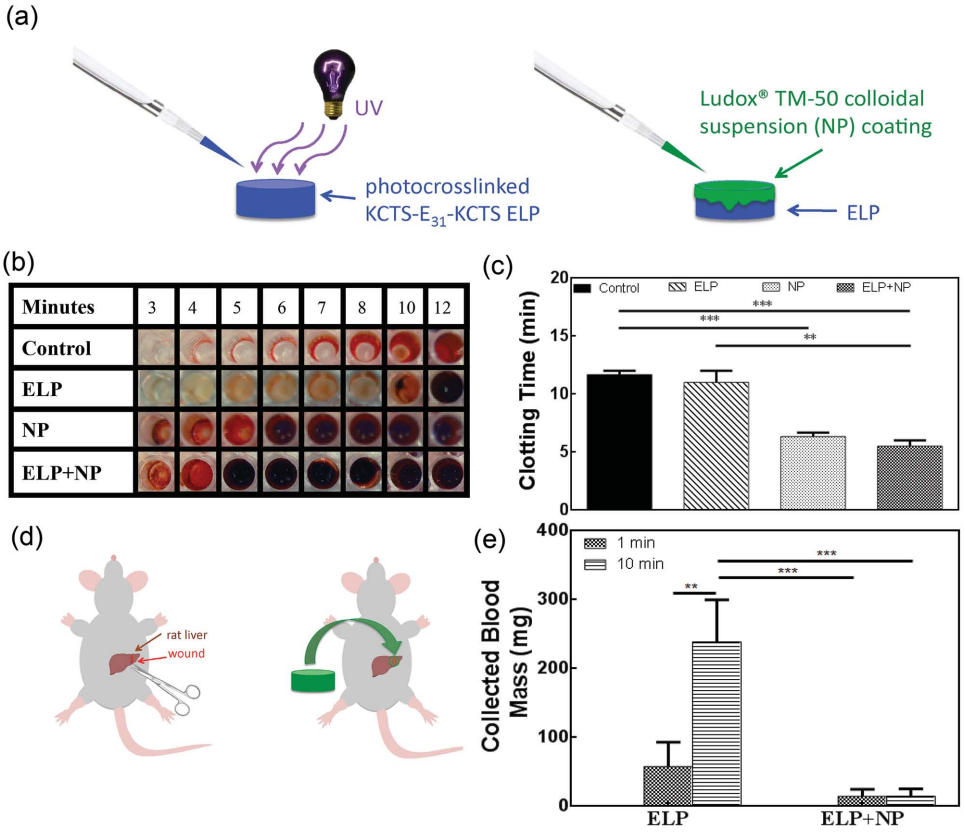

Figure 6. Application of ELP hydrogels combined with silica nanoparticles as hemostats. a) A schematic of coating silica nanoparticle (NP; Ludox TM-50) solutions onto the photocrosslinked ELPs. b) A 96 well plate clotting time assay shows decreased clotting times when NP solutions (10 μL) are combined with the photocrosslinked ELPs (50 μL) (ELP + NP). c) Clotting times measured from the 96 well plate clotting time assay show a significant decrease in clotting time when NP was added. d) A schematic of NP-coated ELP hydrogel placement onto a lethal liver wound. e) In vivo blood loss after application of ELP versus ELP with NP coating showing a significant improvement when NP-coated ELPs are used to treat the wound (**$p < 0.01$, ***$p < 0.001$).

in decreased clotting times in vitro for the photocrosslinked ELPs. A clotting time assay was performed in which wells of a 96-well plate were used to monitor the progression of clot formation.[51] After set times, washing wells containing combinations of activated whole blood and photocrosslinked ELP with or without a silica NP solution coating with saline solution will result in only clotted blood remaining in the well.

Improvement in clotting time upon the addition of NPs highlighted the continued procoagulant activity of silica NP after coating on ELPs. Concentrations as small as 2% (v/v) of NP in whole blood (2 μL in 100 μL whole blood) were able to decrease clotting times compared to controls. Maximum decreases in clotting time were observed with 10% (v/v) of NP in whole blood (10 μL NP in 100 μL whole blood), with a 46% drop in clotting time compared to controls, comparable to commercial hemostats.[51] Photocrosslinked KCTS-E_{31}-KCTS were then coated with 10 μL of NP prior to addition of blood, resulting in a decrease in clotting time of 53% compared to controls (Figure 6b,c). The extended clotting time for the control sample compared to other observed whole blood clotting times[51] is likely due to variability between donors. However, using this time as an internal control, the improvements in clotting time with KCTS-E_{31}-KCTS and NP treatment suggest a synergistic effect on clotting when KCTS-E_{31}-KCTS and NP are used. It is hypothesized that the absorption of NP to polymer chains[59] can concentrate the NP on the ELP surface and focus their nanobridging activity to the interface between the blood and ELP as opposed to the solution of NPs being uniformly mixed in the whole blood.

2.6.2. In Vivo Liver Bleeding Model

When applied in vivo, photocrosslinked ELP samples coated with NP solution promoted hemostasis in standardized liver wounds with acute hemorrhage (Figure 6d) that was otherwise lethal, as demonstrated in a recent publication by the authors.[51] Placement of the photocrosslinked ELP samples on liver wounds resulted in occlusive clotting within 10 min, while the addition of NP to ELP gels decreased the bleeding time to 2 min. NP solutions on the surface of ELP membranes have been shown to promote hemostasis when applied to a bleeding liver wound by the nanobridging process. When NP was coated on the surface of photocrosslinked ELP, improvements in clotting time and blood loss were greater than when photocrosslinked ELP was applied to the wound alone. When ELP and NP were combined in treatment, blood mass loss was 76% and 94% lower after 1 and 10 min, respectively, compared

to treatment with ELP alone (Figure 6e). Similar decreases in blood loss and time to hemostasis have been observed with acrylamide-based particles in liver bleeding models.[60] Additionally, further blood loss was still observed after 10 min when only ELP was applied to liver bleeding while blood loss was only observed for an average of 1.5 min when NP was coated on the ELP surface. Removal of the photocrosslinked hydrogel from the wound did not cause re-bleeding, indicating sufficient sealing of the wound. This ability of the NPs to promote hemostasis when coated on photocrosslinked ELP creates a hemostat system with improved extensibility and stability in vivo. Such systems can be utilized for vascular or soft tissue injuries which require a combination of clotting ability, elasticity, and flexibility to adjust to wounds with complex geometry or moving tissue.[56,57]

3. Conclusion

In conclusion, recombinantly expressed ELP hydrogels were shown to photocrosslink without additional modifications to the canonical amino acid protein sequence. The gels were extensible up to 420% strain and fatigue resistant in compression. In vivo examination revealed excellent biocompatibility and minimal degradation, resulting in early and progressive ingrowth of host tissue. Furthermore, hemostatic functionalization with NPs allowed for effective treatment of a lethal bleeding liver wound. With these qualities, such a photocrosslinkable system has the potential to be used in biomedical applications as a sealant for soft, flexible tissue injuries like in blood vessels, skin, lung, or cardiac tissue.

4. Experimental Section

Protein Synthesis: A modified ELP was engineered by inserting a previously designed ELP sequence into a modified pET-28 plasmid containing Nhe1 and Spe1 restriction enzyme sites as well the amino acid sequence Lys-Cys-Thr-Ser flanking the ELP. First, oligomers encoding for these residues were acquired (Sigma), which had the following nucleotide sequences:

5′ to 3′ gatccaaatgtaccagcgctagcagtgtctaacgactagtaaatgcacgtcttaaa

3′ to 5′ agcttttaagacgtgcatttactagtcgttagacactgctagcgctggtacatttg

This sequence contained BamHI, HindIII, SpeI, and NheI restriction sites. The oligomers were annealed together and ligated into a modified pET vector, cut with BamHI and HindIII. After confirming correct ligation with sequencing, a digest with NheI and SpeI was performed to allow for the insertion of the ELP sequence, E_{22}, also cut from a pET vector with Nhe1 and Spe1. Following ligation, the sequence-confirmed plasmid was transformed into TurnerDE3 expression cells (New England Biolabs). A 50 mL starter culture of the expression *E. coli* cells in LB media was incubated overnight at 37 °C, followed by inoculation of a 5 L fermentation in Terrific Broth. Fermentation was allowed to proceed for 14 h at 30 °C in a custom-designed fermenter. Filtered air was delivered to the culture for appropriate aeration and propellers used for agitation. Cell pellets were initially centrifuged and frozen at −80 °C overnight. The cell pellets were suspended at a concentration of 100 mL buffer per 30 g cell pellet mass, on ice, in buffer (100×10^{-3} M Tris, 100×10^{-3} M NaCl, 5×10^{-3} M $MgCl_2$, 1×10^{-3} M EDTA, 14.3×10^{-3} M BME adjusted to pH = 7.5. lysozyme (1 mg mL^{-1} buffer) was added for 30 min followed by sonication. The solution was then purified by inverse transition cycling (ITC). The solution was centrifuged at 4 °C and the supernatant was decanted from the pelleted cell debris. DNase and RNase were added to the supernatant and the solution was incubated at 37 °C for 1 h. The solution was centrifuged for 1 h at 37 °C and the supernatant was decanted from the pelleted ELPs, which were suspended in cold buffer and allowed to dissolve at 4 °C overnight. The process was continued, with aliquots taken of each supernatant after spinning at hot (37 °C) and cold (4 °C) temperatures for analysis by denaturing SDS-PAGE, stained with Coomassie Blue dye. After ITC, the buffered solution was dialyzed against 4 L of water for 21 h, exchanging the water every 3 h. Dialyzed solutions were then freeze dried and stored in sealed centrifuge tubes until use.

Hydrogel Fabrication: Lyophilized ELP was dissolved in phosphate-buffered saline (PBS, Life Technologies) containing 0.5% (w/v) 2-hydroxy-1-(4-(hydroxyethoxy) phenyl)-2-methyl-1-propanone (Irgacure® 2959, CIBA Chemicals). To avoid coacervation and precipitation of ELP prior to crosslinking, ELP solutions at defined concentrations were mixed and stored on ice, and only brought to room temperature just before crosslinking. 90 µL of ELP solution was placed in pre-manufactured polydimethylsiloxane (PDMS) molds ($15 \times 6 \times 1$ mm). Solutions were photocrosslinked with UV exposure (80 mm sample–source distance, OmniCure S2000, 360–480 nm wavelength, 850 mW) for 3 min. Samples were then collected from the molds and detached after soaking in PBS for 2 min to ensure easy removal from the mold.

Reduced Protein Gel: A 10% (w/v) photocrosslinked ELP gel was incubated in a 30×10^{-3} M tris (2-carboxyethyl) phosphine hydrochloride (TCEP) solution overnight at room temperature to reduce all disulfide bonds. The TCEP concentration was a fivefold molar excess relative to the concentration of cysteine residues. A small solid portion remained after this reduction but the rest of the gel was completely dissolved into the TCEP solution. The resulting solution containing the dissolved gel proteins and TCEP was then dialyzed against pure water, lyophilized, and mixed with a Coomassie Blue loading dye containing 30×10^{-3} M TCEP. Samples were loaded and run on a 12% (w/v) SDS-polyacrylamide gel at 200 V for 40 min. The polyacrylamide gel was stained in Coomassie Blue R-250 staining dye and destained in destaining solution (50 vol% double distilled water, 40 vol% ethanol, and 10 vol% acetic acid).

Scanning Electron Microscopy (SEM): Photocrosslinked ELP hydrogel samples were lyophilized and mounted on aluminum holders. A 30 nm thick gold layer was sputter coated on all samples prior to imaging. SEM images were obtained by using a FEI/Philips XL30 FEG SEM at 15 kV. ImageJ software was used to calculate the apparent pore size of the ELP hydrogels. Triplicates of 10%, 15%, and 20% samples were imaged and pores were selected per image for pore size measurements ($n = 90$).

Swelling Ratio: The swelling ratios of 10%, 15%, and 20% (w/v) ELP hydrogels were evaluated in PBS at 4 °C and 37 °C. Swelling tests were performed as previously reported.[18,61] Briefly, 90 µL of ELP solution was injected into a PDMS mold with a 7 mm diameter and 5 mm depth. The prepolymer solution was exposed to UV light for 3 min. Hydrogels were lyophilized and dry weights were recorded. Next, samples were placed in PBS for different time points (4, 12, 24, 48 h) at 4 °C or 37 °C. At each time point, samples were removed from PBS and weighed. The swelling ratio was calculated following the equation: $(W_{wet}–W_{dry})/W_{dry} \times 100\%$, where W_{dry} is the weight after lyophilizing and W_{wet} is after removal from PBS. Tests were performed at least in triplicate for each condition.

Mechanical Characterization: Tensile and compressive cyclic testing of ELP hydrogels were performed using a mechanical tester (Instron model 5542) with a 10 N load cell. Gels were photocrosslinked as previously described (dimensions $15 \times 5 \times 1$ mm) for tensile tests. Gels were then incubated in PBS for 4 h at 37 °C prior to mechanical testing. We performed the mechanical testing on the samples prior to reaching maximum swelling ratio to mimic the swelling state of ELP when applying as a tissue sealant. ELP tissue sealant will not be immersed in solution prior to application; therefore, it will not be fully swollen. The dimensions of the samples were measured with a digital caliper. To minimize dehydration during testing, a humidifier was used surrounding the testing apparatus. The strain rate was 10 mm min^{-1} and performed until sample failure. Ultimate tensile stress (stress obtained at the

failure point), maximum strain (strain obtained at the failure point), and elastic modulus (the slope of the stress–strain curve) were determined, with samples taken in triplicate for each condition.

Compression Test: Compressive samples were prepared in the same molds used for swelling tests (7 mm in diameter and 5 mm in depth). Prior to the test, hydrogels were incubated in PBS for 4 h. The compressive strain rate was 10 mm min^{-1} and strain level was up to ≈70% of the original height. The compression and load were recorded for 10 cycles, after which there was no significant change in the curve shape. The compressive modulus was obtained from the slope during loading on the 8th cycle (the slope of the stress–strain curve, taken from the 0.1–0.3 mm mm^{-1} of the strain).The energy loss was calculated for the 8th cycle based on the area between the loading and unloading curves, following the equation

$$\text{Energy Loss} = \frac{\text{Area below loading} - \text{Area below unloading}}{\text{Area below loading}} \times 100\%$$

Samples were tested in triplicate for each condition.

Cell Culture: Mesenchymal stem cells (MSC, from Lonza) and human umbilical vein endothelial cells (HUVECs, American Type Culture Collection (ATCC)) were used for in vitro studies. MSCs were cultured in mesenchymal stem cell growth medium (MSC-GM, Lonza) with 10% fetal bovine serum (FBS, Invitrogen), glutamine-penicillin-streptomycin (GPS, Invitrogen). HUVECs were cultured in endothelial basal medium (EBM-2, Lonza) enriched with endothelial growth factors (BulletKit, Lonza) and 100 units mL^{-1} penicillin-streptomycin (Gibco, USA). MSCs and HUVECs were cultured in 5% CO_2 humidified incubators at 37 °C. Cells were passaged every 3 days and media changed every other day.

In Vitro 2D Cell Studies: 10 mL 10% (w/v) ELP solutions were photocrosslinked on 3-(trimethoxysilyl)propyl methacrylate (TMSPMA) coated glass slice with 150 μm spacers for 30 s. Cells were then seeded on the top of the ELP gels placed in a 24 well plate. The cell seeding density was 1×10^4 cell per well. Cell viability and proliferation were studied on days 1, 4, and 7 of culture. Media was changed every other day.

Cell Viability: Cell viability was performed with the Live/Dead kit (Invitrogen, USA) following instructions from the manufacturer. Briefly, ethidium homodimer-1 (2 μl mL^{-1}) and calcein AM (0.5 μL mL^{-1}) were mixed in PBS. After that, the well plate was incubated for 15 min at 37 °C and imaged with an inverted fluorescence microscope (Nikon TE 2000-U, Nikon instruments Inc., USA). ImageJ was used to count the live and dead cells by using at least four images from different areas of three hydrogels for each ELP condition. Cell viability was calculated by division of the number of live cells by the total number of stained cells.

Cell Activity: Cell activity was measured with PrestoBlue cell viability reagents (Life Technologies) following the manufacturer's protocol. Each construct was incubated with 400 μL of a solution containing 10% PrestoBlue reagent and 90% respective cell media (MSC-GM media for MSCs and EBM-2 for HUVECs) for 2 h at 37 °C. The resulting fluorescence was measured at a wavelength of 560 nm (excitation) and 590 nm (emission) with a fluorescence reader (Synergy HT-Reader, BioTek, Winooski, VT). By subtracting the fluorescence values from the control wells without cells, the relative fluorescence values were calculated and plotted for each day, where higher fluorescence values correlate to greater total metabolic activity. Samples were tested in triplicate for each condition.

Cell Spreading: Phalloidin (Invitrogen) and 4,6-diamidino-2-phenylindole (DAPI; Sigma) staining was used to investigate cellular attachment and spreading on the surfaces of ELP hydrogels. To stain F-actin of the cell, the cells were permeabilized in a 0.1% (w/v) Triton solution in PBS for 30 min and blocked in 1% (w/v) bovine serum albumin (BSA) for 1 h. The samples were then incubated in a solution of 1:40 ratio of phalloidin with 0.1% BSA for 45 min at room temperature to perform the actin cytoskeleton staining. For DAPI staining, the samples were incubated in a 0.1% (v/v) DAPI solution in PBS for 10 min at 37 °C to stain the cell nuclei. The stained samples were then washed three times with PBS before visualizing with an inverted fluorescence microscope.

In Vitro Enzymatic Degradation: UV crosslinked gels were made as previously described for swelling tests. The samples were freeze dried and dry weights were recorded. Next, samples were equilibrated in PBS (Life Technologies) and then incubated with the digestion enzyme Proteinase K (Sigma) at 0.5 U mL^{-1} in PBS for 6 h. Finally, samples were lyophilized and dry weights were recorded again. The percentage of hydrogel loss was the difference between the initial and the final dry weight divided by the initial weight.

In Vitro Clotting Tests: Citrated human blood was mixed with 0.1 M $CaCl_2$ at a ratio of 9:1 to reverse anticoagulation. Following mixing by pipetting for 1–2 s, 100 μL was aliquoted into 96 well plates with bottoms coated in either Ludox TM-50 (Sigma) colloidal nanoparticle suspension (labelled Ludox), 50 μL of 10% (w/v) photocrosslinked KCTS-E_{31}-KCTS (labeled ELP), 50 μL of 10% (w/v) photocrosslinked KCTS-E_{31}-KCTS with 10 μL Ludox TM-50 pipetted on the surface (labeled ELP + NP), or uncoated well plates (labeled Control). At selected time points, individual wells were rinsed with 9 mg mL^{-1} saline solution and the liquid aspirated until the solution remained clear, indicating removal of all soluble blood components, and leaving behind only clotted blood. The clotting time was marked as the well in which a uniform clot covered the entire bottom of the well plate.

Animal Experiments: For all animal experiments, male Wistar rats weighing 200–250 g were obtained from Charles River (Wilmington, MA, USA) and housed in the local animal care facility of the Partners Research Building (Cambridge, MA, USA) under conditions of circadian day–night rhythm and feeding ad libitum. Anesthesia was achieved by isoflurane inhalation (2.0%–2.5%). All experiments were conducted according to the NIH "Guide for the Care and Use of Laboratory Animals," and approved by the local animal care committee (HMA Standing Committee on Animals; Protocol No. 05055).

Subcutaneous Implants: The medio-dorsal skin of rats was incised by 1 cm in length and a small lateral subcutaneous pocket was bluntly prepared. ELP samples (n = 20; 1 × 5 mm disks) were thoroughly implanted under sterile conditions before anatomical wound closure and recovery from anesthesia. At days 3, 14, 28, and 56, euthanization by CO_2 inhalation was followed by explantation of the ELP samples including the adjacent tissue. Afterward, the samples were processed for histological analyses and degradation studies.

Histology and Immunohistology: Histological analyses were performed on 6 μm cryo-sections of the explanted ELP samples. After fixation with paraformaldehyde, hematoxylin, and eosin staining was conducted as previously reported.[62] Immunohistological staining was performed as previously reported.[63] As primary antibodies, anti-CD3 and anti-CD68 (Abcam, Cambridge, MA, USA) were used, and secondary antibodies were Alexa Fluor-conjugated (Invitrogen, Carlsbad, USA). Sections were covered with DAPI-enriched Vectashield mounting medium (Vector Labs, Peterborough, United Kingdom) and visualized on an Axio Observer microscope (Zeiss, Jena, Germany).

In Vivo Liver Bleeding: A median laparotomy was performed and the central liver lobe was visualized by retraction of skin. A 0.5 cm cut was made through the edge of the lobe with straight operating scissors. After removing hemorrhaged blood with dry filter paper, photocrosslinked KCTS-E_{31}-KCTS samples (n = 3 animals; 90 μL of 10% (w/v) KCTS-E_{31}-KCTS, 0.5% photoinitiator crosslinked for 180 s) were deposited on the wound with a spatula. Additional samples had Ludox TM-50 solution (20 μL) added to the top and bottom of KCTS-E_{31}-KCTS photocrosslinked samples (n = 3 animals). These were added to the wounds in the same way as KCTS-E_{31}-KCTS samples. After application of the hydrogel, lost blood was absorbed on filter papers for later mass quantification until bleeding ceased. Following this observation, the time was marked and the crosslinked sample was removed to test for subsequent bleeding. Rats were then sacrificed by severing of the aorta.

Statistical Analysis: Data were compared using one-way or two-way ANOVA methods, depending on the variables in the data set, in

GraphPad Prism 6. Data are expressed as means ± standard deviation (SD) of measurements (*$p < 0.05$, **$p < 0.01$ and ***$p < 0.001$).

Supporting Information

Supporting Information is available from the Wiley Online Library or from the author.

Acknowledgements

Y.-N.Z., R.K.A., and Q.V.-M. contributed equally to this work. Y.-N.Z., R.K.A., and Q.V.-M. designed, performed, and analyzed experiments. Q.V.-M., A.A., A.V., and N.A. performed and analyzed in vivo experiments. Y.-N.Z., R.K.A., and Q.V.-M. wrote the manuscript. A.A., A.V., A.M., B.D.O., A.K., and N.A. analyzed experiments and provided comments to the manuscript. R.K.A. was supported by a National Institutes of Health (NIH) Interdepartmental Biotechnology Training Program (NIH/NIGMS 5T32GM008334). This research was supported by the U.S. Army Research Office under contract W911NF-13-D-0001. A.A. acknowledges postdoctoral funding from the German Heart Foundation, Frankfurt, Germany. The authors (A.M., A.K.) would like to thank the National Plan for Science, Technology and Innovation (MAARIFAH) by King Abdulaziz City for Science and Technology, Grant No. 12-MED3096-3 for their support and funding of this project. A.K. acknowledges funding from the National Science Foundation (EFRI-1240443), IMMODGEL (602694), and the National Institutes of Health (EB012597, AR057837, DE021468, HL099073, AI105024, and AR063745).

Received: April 13, 2015
Revised: May 24, 2015
Published online: July 1, 2015

[1] K. Y. Lee, D. J. Mooney, *Chem. Rev.* **2001**, *101*, 1869.
[2] a) S. Böttcher-Haberzeth, T. Biedermann, E. Reichmann, *Burns* **2010**, *36*, 450; b) E. S. Place, N. D. Evans, M. M. Stevens, *Nat. Mater.* **2009**, *8*, 457.
[3] J. Zhu, R. E. Marchant, *Expert Rev. Med. Devices* **2011**, *8*, 607.
[4] B. P. Chan, T. Y. Hui, O. C. Chan, K. F. So, W. Lu, K. M. Cheung, E. Salomatina, A. Yaroslavsky, *Tissue Eng.* **2007**, *13*, 73.
[5] J. L. Drury, D. J. Mooney, *Biomaterials* **2003**, *24*, 4337.
[6] A. S. Hoffman, *Adv. Drug Delivery Rev.* **2002**, *54*, 3.
[7] S. R. MacEwan, A. Chilkoti, *Biopolymers* **2010**, *94*, 60.
[8] a) W. E. Hennink, C. F. van Nostrum, *Adv. Drug Delivery Rev.* **2012**, *64*, 223; b) V. Charulatha, A. Rajaram, *Biomaterials* **2003**, *24*, 759.
[9] A. Nicol, D. C. Gowda, D. W. Urry, *J. Biomed. Mater. Res.* **1992**, *26*, 393.
[10] C. Chou, R. Uprety, L. Davis, J. W. Chin, A. Deiters, *Chem. Sci.* **2011**, *2*, 480.
[11] I. S. Farrell, R. Toroney, J. L. Hazen, R. A. Mehl, J. W. Chin, *Nat. Methods* **2005**, *2*, 377.
[12] J. L. Ifkovits, J. A. Burdick, *Tissue Eng.* **2007**, *10*, 2369.
[13] J. Raphel, A. Parisi-Amon, S. C. Heilshorn, *J. Mater. Chem.* **2012**, *22*, 19429.
[14] M. Martino, A. M. Tamburro, *Biopolymers* **2001**, *59*, 29.
[15] a) M. J. B. Wissink, R. Beernink, J. S. Pieper, A. A. Poot, G. H. M. Engbers, T. Beugeling, W. G. van Aken, J. Feijen, *Biomaterials* **2001**, *22*, 151; b) L. Huang, R. A. McMillan, R. P. Apkarian, B. Pourdeyhimi, V. P. Conticello, E. L. Chaikof, *Macromolecules* **2000**, *33*, 2989.
[16] M. K. McHale, L. A. Setton, A. Chilkoti, *Tissue Eng.* **2005**, *11*, 1768.
[17] A. K. Gaharwar, C. Rivera, C.-J. Wu, B. K. Chan, G. Schmidt, *Mater. Sci. Eng. C* **2013**, *33*, 1800.
[18] N. Annabi, S. M. Mithieux, P. Zorlutuna, G. Camci-Unal, A. S. Weiss, A. Khademhosseini, *Biomaterials* **2013**, *34*, 5496.
[19] B.-S. Chiou, R. J. English, S. A. Khan, *Macromolecules* **1996**, *29*, 5368.
[20] D. L. Nettles, A. Chilkoti, L. A. Setton, *Adv. Drug Delivery Rev.* **2010**, *62*, 1479.
[21] D. L. Nettles, K. Kitaoka, N. A. Hanson, C. M. Flahiff, B. A. Mata, E. W. Hsu, A. Chilkoti, L. A. Setton, *Tissue Eng. Part A* **2008**, *14*, 1133.
[22] C. Baldock, A. F. Oberhauser, L. Ma, D. Lammie, V. Siegler, S. M. Mithieux, Y. Tu, J. Y. H. Chow, F. Suleman, M. Malfois, S. Rogers, L. Guo, T. C. Irving, T. J. Wess, A. S. Weiss, *Proc. Natl. Acad. Sci. U.S.A.* **2011**, *108*, 4322.
[23] D. E. Meyer, A. Chilkoti, *Nat. Biotechnol.* **1999**, *17*, 1112.
[24] H. Betre, L. A. Setton, D. E. Meyer, A. Chilkoti, *Biomacromolecules* **2002**, *3*, 910.
[25] S. C. Heilshorn, J. C. Liu, D. A. Tirrell, *Biomacromolecules* **2005**, *6*, 318.
[26] X. X. Xia, Q. Xu, X. Hu, G. Qin, D. L. Kaplan, *Biomacromolecules* **2011**, *12*, 3844.
[27] K. Trabbic-Carlson, L. A. Setton, A. Chilkoti, *Biomacromolecules* **2003**, *4*, 572.
[28] a) H. Wang, L. Zhou, J. Liao, Y. Tan, K. Ouyang, C. Ning, G. Ni, G. Tan, *J. Mater. Sci.: Mater. Med.* **2014**, *25*, 2173; b) R. A. McMillan, V. P. Conticello, *Macromolecules* **2000**, *33*, 4809.
[29] K. Zhang, M. R. Diehl, D. A. Tirrell, *J. Am. Chem. Soc.* **2005**, *127*, 10136.
[30] K. Nagapudi, W. T. Brinkman, J. E. Leisen, L. Huang, R. A. McMillan, R. P. Apkarian, V. P. Conticello, E. L. Chaikof, *Macromolecules* **2002**, *35*, 1730.
[31] S. Tang, M. J. Glassman, S. Li, S. Socrate, B. D. Olsen, *Macromolecules* **2014**, *47*, 791.
[32] G. Odian, *Principles Of Polymerization*, Wiley-Interscience, Hoboken, NJ, USA **2004**.
[33] F. Dénès, M. Pichowicz, G. Povie, P. Renaud, *Chem. Rev.* **2014**, *114*, 2587.
[34] C. L. Hawkins, M. J. Davies, *Biochim. Biophys. Acta* **2001**, *1504*, 196.
[35] M. J. Davies, *Arch. Biochem. Biophys.* **1996**, *336*, 163.
[36] N. Annabi, J. W. Nichol, X. Zhong, C. Ji, S. Koshy, A. Khademhosseini, F. Dehghani, *Tissue Eng. Part B* **2010**, *16*, 371.
[37] N. Annabi, A. Tamayol, J. A. Uquillas, M. Akbari, L. E. Bertassoni, C. Cha, G. Camci-Unal, M. R. Dokmeci, N. A. Peppas, A. Khademhosseini, *Adv. Mater.* **2014**, *26*, 85.
[38] D. W. Lim, D. L. Nettles, L. A. Setton, A. Chilkoti, *Biomacromolecules* **2007**, *9*, 222.
[39] a) D. He, M. Miao, E. E. Sitarz, L. D. Muiznieks, S. Reichheld, R. J. Stahl, F. W. Keeley, J. Parkinson, L. Kreplak, *PLoS One* **2012**, *7*, 1; b) M. Miao, E. Sitarz, C. M. Bellingham, E. Won, L. D. Muiznieks, F. W. Keeley, *Biopolymers* **2013**, *99*, 392.
[40] T. S. Wheeler, N. D. Sbravati, A. V. Janorkar, *Ann. Biomed. Eng.* **2013**, *41*, 2042.
[41] a) H. Kamata, Y. Akagi, Y. Kayasuga-Kariya, U.-i. Chung, T. Sakai, *Science* **2014**, *343*, 873; b) J.-Y. Sun, X. Zhao, W. R. K. Illeperuma, O. Chaudhuri, K. H. Oh, D. J. Mooney, J. J. Vlassak, Z. Suo, *Nature* **2012**, *489*, 133.
[42] F. A. Saleh, M. Whyte, P. G. Genever, *Eur. Cell Mater.* **2011**, *22*, 242.
[43] H. J. Park, Y. Zhang, S. P. Georgescu, K. L. Johnson, D. Kong, J. B. Galper, *Stem Cell Rev.* **2006**, *2*, 93.
[44] K. Ito, T. Suda, *Nat. Rev. Mol. Cell Biol.* **2014**, *15*, 243.
[45] S. Baranoski, *Nursing* **2008**, *38*, 60.
[46] R. R. Costa, C. A. Custódio, A. M. Testera, F. J. Arias, J. C. Rodríguez-Cabello, N. M. Alves, J. F. Mano, *Adv. Funct. Mater.* **2009**, *19*, 3210.
[47] S. Baranoski, *Nursing* **2008**, *38*, 14.

[48] W. Xiao, J. He, J. W. Nichol, L. Wang, C. B. Hutson, B. Wang, Y. Du, H. Fan, A. Khademhosseini, *Acta Biomater.* **2011**, *7*, 2384.
[49] D. W. Urry, T. M. Parker, M. C. Reid, D. C. Gowda, *J. Bioact. Compat. Polym.* **1991**, *6*, 263.
[50] C. Hrabchak, J. Rouleau, I. Moss, K. Woodhouse, M. Akens, C. Bellingham, F. Keeley, M. Dennis, A. Yee, *Acta Biomater.* **2010**, *6*, 2108.
[51] A. K. Gaharwar, R. K. Avery, A. Assmann, A. Paul, G. H. McKinley, A. Khademhosseini, B. D. Olsen, *ACS Nano* **2014**, *8*, 9833.
[52] W. D. Spotnitz, *ISRN Surg.* **2014**, *2014*, 28.
[53] L. Med, *Market Diligence* **2012**.
[54] a) S. Ghanaati, I. Willershausen, M. Barbeck, R. Unger, M. Joergens, R. Sader, C. Kirkpatrick, B. Willershausen, *European J. Med. Res.* **2010**, *15*, 483; b) T. M. Shazly, A. B. Baker, J. R. Naber, A. Bon, K. J. Van Vliet, E. R. Edelman, *J. Biomed. Mater. Res., Part A* **2010**, *95A*, 1159.
[55] A. C. van Der Ham, W. J. Kort, I. M. Weijma, H. F. G. M. D. Van Ingh, J. Jeekel, *Br. J. Surg.* **1991**, *78*, 49.
[56] W. D. Spotnitz, S. Burks, *Transfusion* **2008**, *48*, 1502.
[57] W. D. Spotnitz, *World J. Surg.* **2010**, *34*, 632.
[58] A. Meddahi-Pellé , A. Legrand, A. Marcellan, L. Louedec, D. Letourneur, L. Leibler, *Angew. Chem. Int. Ed.* **2014**, *53*, 6369.
[59] S. Rose, A. Prevoteau, P. Elziere, D. Hourdet, A. Marcellan, L. Leibler, *Nature* **2014**, *505*, 382.
[60] A. M. Behrens, M. J. Sikorski, T. Li, Z. J. Wu, B. P. Griffith, P. Kofinas, *Acta Biomater.* **2014**, *10*, 701.
[61] N. Annabi, S. M. Mithieux, A. S. Weiss, F. Dehghani, *Biomaterials* **2009**, *30*, 1.
[62] A. Assmann, K. Zwirnmann, F. Heidelberg, F. Schiffer, K. Horstkotter, H. Munakata, F. Gremse, M. Barth, A. Lichtenberg, P. Akhyari, *Biomaterials* **2014**, *35*, 7416.
[63] A. Assmann, C. Delfs, H. Munakata, F. Schiffer, K. Horstkotter, K. Huynh, M. Barth, V. R. Stoldt, H. Kamiya, U. Boeken, A. Lichtenberg, P. Akhyari, *Biomaterials* **2013**, *34*, 6015.